remote sensing

MDPI

Article

Complementarity Characteristics of Actual and Potential Evapotranspiration and Spatiotemporal Changes in Evapotranspiration Drought Index over Ningxia in the Upper Reaches of the Yellow River in China

Huihui Liu [1,2], Dongdong Song [3,*], Jinling Kong [1], Zengguang Mu [4], Xixuan Wang [1], Yizhu Jiang [5] and Jingya Zhang [1]

[1] College of Geological Engineering and Geomatics, Chang'an University, Xi'an 710054, China
[2] Institute of Natural Resources Survey of Ningxia, Yinchuan 750002, China
[3] School of Public Administration, China University of Geosciences (Wuhan), Key Laboratory of Rule of Law Research, Ministry of Natural Resources, Wuhan 430074, China
[4] Natural Resources Information Center of Ningxia, Yinchuan 750002, China
[5] College of Earth Sciences and Resources, Chang'an University, Xi'an 710054, China
* Correspondence: songdd@cug.edu.cn

Abstract: Based on energy balance theory, using Theil–Sen median trend analysis and the Mann–Kendall test, this research studied the applicability of the complementary theory of evapotranspiration (ET) over Ningxia in the Upper Reaches of the Yellow River with MOD16 ET product and the measured data of meteorological stations, based on which ET drought index (EDI) was proposed for the first time. Moreover, the usability of EDI was also verified and its influencing factors were analyzed. The results revealed that there was a complementary relationship between AET and PET in 91.1% of the area in Ningxia, including strictly complementary and asymmetrically complementary relationships in 69.2% and 21.9% of the total area, respectively. EDI ranged from 0 to 1 and was useful to accurately reflect the degree of drought of the study area on the annual and monthly scales. From 2001 to 2020, the average annual EDI was 0.66, and the smallest monthly EDI was in January and the largest was in May. EDI of different time scales had different influencing factors. Precipitation was the most influencing factor of annual EDI, but the influencing factors of monthly EDI was different over time. However, surface non-precipitation water replenishment, such as irrigation, had great impact both on annual EDI and monthly EDI. The application scope of the theory of ET complementarity was extended to the study area for the first time, and EDI was proposed and applied, which will provide a theoretical basis and empirical reference for drought research based on ET data in arid and semi-arid areas.

Keywords: complementary relationship of evapotranspiration; evapotranspiration drought index (EDI); Ningxia

Citation: Liu, H.; Song, D.; Kong, J.; Mu, Z.; Wang, X.; Jiang, Y.; Zhang, J. Complementarity Characteristics of Actual and Potential Evapotranspiration and Spatiotemporal Changes in Evapotranspiration Drought Index over Ningxia in the Upper Reaches of the Yellow River in China. *Remote Sens.* **2022**, *14*, 5953. https://doi.org/10.3390/rs14235953

Academic Editor: Guido D'Urso

Received: 21 October 2022
Accepted: 20 November 2022
Published: 24 November 2022

1. Introduction

Surface evapotranspiration (ET) is an important part of the water cycle and one of the most important processes in matter and energy exchange between the land surface and the atmosphere [1]. ET is also a central link in the climate system, which is the foundation of the studies of crop water demand estimation, irrigation water use efficiency, ecological process analysis, and regional drought assessment [2].

Studies on the relationship between actual ET (AET) and potential ET (PET) play a very important role in analyzing the interaction between climate and hydrology [3]. AET is the actual water consumed by evaporation and transpiration on the unsaturated surface, which is often assumed to be a function of evaporation capacity and surface water content. PET is the maximum evaporation capacity of the underlying surface under the condition

of full water supply. However, different theories provide different explanations for the relationship between AET and PET. Penman [4] showed via the proportional hypothesis theory that AET was proportional to PET, and the rate depended on the availability of water under insufficient water supply. Based on the theory of energy balance, Bouchet [5] proposed via complementary correlation theory that if the total energy was kept constant, PET would decrease when soil moisture decreased, and the residual energy originally used for AET would be used to increase PET, and the rate of AET increase (or decrease) was equal to that of PET. Formally, the proportional hypothesis theory and the complementary correlation theory are completely contrary, so the relationship between AET and PET in a particular region can only conform to one of the theories. Cohen et al. [6] found that the complementarity theory of ET was most applicable to arid regions, and the proportional hypothesis theory was mostly suitable for applications in humid regions, which still needed to be tested in wider regions.

Northwest China is a part of the arid region in central Asia and one of the most sensitive regions to global climate change [7]. In recent years, a large number of studies have been conducted on ET in the arid and semi-arid regions of northwest China [8–12]. Some scholars reported a strong correlation between the variation in ET and that in precipitation and vegetation type in northwest arid areas over the past 15 years. Others showed that annual ET was high in the north and low in the south of the Yellow River source region from 1979 to 2014. Some scholars reported that PET showed an upward trend, and the maximum temperature was the most important meteorological factor affecting ET in the Gansu section of the Yellow River Basin. The abovementioned studies focused only on the trend of variation in ET and the effect of meteorological factors on ET in arid areas, without considering the relationship between AET and PET and their effect on ET. Thus, the degree of regional drought and its changing trend could not be directly revealed by ET.

The use of remote sensing (RS) technology to study ET not only reflects the spatial heterogeneity of ET but also meets the needs of global and regional ET research. The global MODIS ET dataset was developed by the Numerical Terradynamic Simulation Group at the University of Montana, USA. This dataset is widely used to study ET with high spatiotemporal resolution. Kim et al. [13] verified the MODIS ET product using vorticity covariance data from 17 stations of the Asian flux network. Liu et al. [14] verified the good applicability of the MODIS ET product in Asia, specifically China, by examining the hydrological and meteorological data. He et al. [15] verified the availability of the MODIS ET product using data obtained from the China Terrestrial Ecosystem Flux Observation and Research Network and using hydrological data, and showed that the MODIS ET product exhibits high simulation accuracy in the Yellow River Basin.

Global Precipitation Measurement (GPM) is a new generation global satellite precipitation measurement program. Dong et al. [16] showed that there was a high consistency between GPM IIMEGR and the rainfall measured data of 76 meteorological stations in the Yellow River Basin. Meng C et al. [17] systematically evaluated the accuracy of GPM IMERG in the source area of the Yellow River, and the results showed that GPM IMERG could well reflect the spatial distribution of precipitation. Using the four evaluation indicators and the extreme precipitation index and error analysis method, based on the precipitation data of the Yellow River Basin rain gauge network, Li Yuanyuan et al. [18] found that there were differences in different regions of the Yellow River Basin, but the overall applicability and accuracy of GPM IIMEGR were high. Therefore, GPM IMERG is used as precipitation observations in this study. Based on MODIS products, GPM IMEGR and the regional meteorological station data collected from 2001 to 2020 in Ningxia, this study is aimed at:

(1). revealing the complementary relationship between AET and PET;
(2). analyzing the internal relation between drought and ET by putting forward the physical significance and model of ET drought index (EDI), quantifying the degree of drought by using EDI and verifying the validity of EDI;
(3). analyzing the variation trends of annual and monthly EDI and the influencing factors.

2. Materials and Methods

2.1. Study Area

Located in the upper reaches of the Yellow River, the Ningxia Hui Autonomous Region (Ningxia) is the only province in China that completely belongs to the Yellow River Basin. The Yellow River flows into Zhongwei and out of Shizuishan, and spans a total length of 397 km in Ningxia [19]. Ningxia covers a total area of 66,400 km^2. The terrain from the north to south of Ningxia is long and narrow, with 456 km between north and south and 250 km between east and west. Ningxia has an average altitude of 1090–2000 m. The elevation gradually decreases from south to north and is divided into the Liupan Mountain, Loess Plateau, Ordos Plateau, Ningxia plain and Helan Mountain. Ningxia is the most sunshine-abundant and severe drought-affected area in China [20]. The mean annual temperature is 8 °C and the annual sunshine period is 3000 h. The average annual precipitation is 289 mm, which mostly occurs from July to September, and the average annual PET is 1585 mm, which is the most sunshine-abundant regions in China. Moreover, Ningxia is one of the most severe drought-affected areas in China [20]. This obvious difference between annual precipitation and annual PET is mainly caused the fact that Ningxia is located in the arid and semi-arid areas. Additionally, the distribution of water resources in Ningxia is extremely unbalanced. Most of the water resources serve the Yellow River irrigation area in north Ningxia, which is one of the 12 commercial grain bases in China with an area of approximately 8600 km^2 [21] (Figure 1). The central arid area of Ningxia has the most limited water resources and surface water. However, water resources are relatively more abundant in the semi-arid and semi-humid mountainous regions of Ningxia in the south.

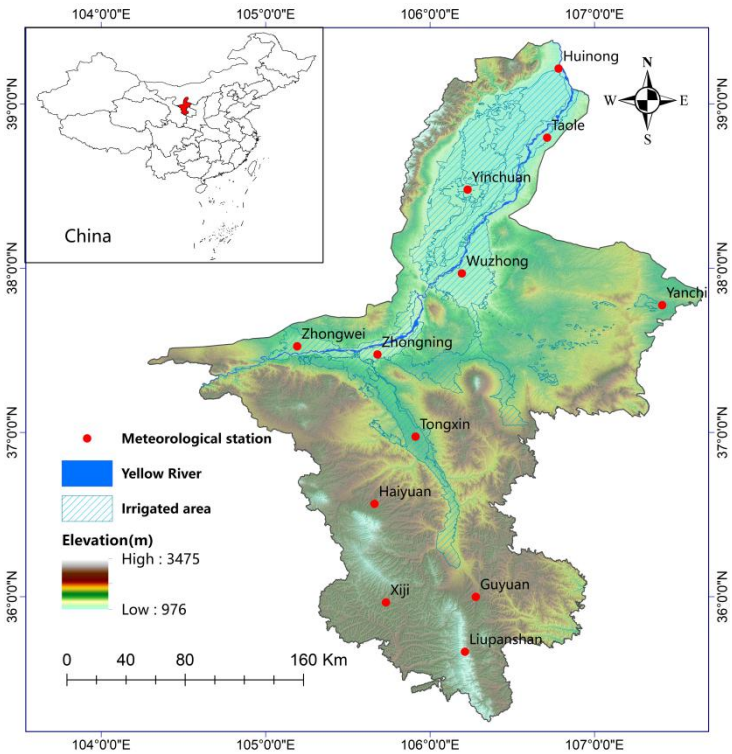

Figure 1. Geographical location and terrain of Ningxia.

2.2. Materials

2.2.1. MODIS ET Product

The MODIS ET project is a part of the NASA/EOS project aimed to estimate global terrestrial ET from the earth land surface using satellite RS data. MOD16A2 and MOD16A3 were the main data resources used in this study, and were downloaded from the NASA Goddard Earth Sciences Data and Information Services Center website (https://modis.gsfc.

nasa.gov/data/dataprod/mod16.php (accessed on 1 May 2022)). MOD16A2—as Version 6.1 of the ET product—is an 8-day synthetic dataset with a spatial resolution of 500 m and is mainly used for the synthesis of the monthly AET and PET dataset. MOD16A3, a Version 6.1 edition, is the annual AET and PET synthesis dataset with a spatial resolution of 500 m. The MODIS reprojection tool (MRT) was used to perform the batch processing of data format conversion and projection transformation; the Python program code was used for data synthesis; and the ArcGIS software was used for clipping. After data processing, the monthly and annual PET and AET data within the study area were obtained.

2.2.2. MODIS Vegetation Index Product

NDVI is one of the important parameters to reflect crop growth and nutrition information. In this study, the NDVI dataset was obtained from MOD13A3, which had a temporal resolution of 1 month and a spatial resolution of 1000 m. The data were obtained from the NASA Goddard Earth Sciences Data and Information Services Center website (https://modis.gsfc.nasa.gov/data/dataprod/mod13.php (accessed on 1 May 2022)). MRT was used for data format conversion and projection transformation, the Python program code was used for annual data synthesis, and ArcGIS software was used for cutting and resampling the spatial resolution to 500 m. With data processing, the monthly and annual NDVI data within the study area were obtained.

2.2.3. MODIS Land Surface Temperature Product

As the input data for calculating the temperature and vegetation drought index, land surface temperature and NDVI had a direct impact on soil moisture and ET. In this study, daytime and nighttime surface temperatures were obtained from MOD11A2, with a temporal resolution of 8 days and a spatial resolution of 1000 m, and were downloaded from the NASA Goddard Earth Sciences Data and Information Services Center website (https://modis.gsfc.nasa.gov/data/dataprod/mod11.php (accessed on 1 May 2022)). MRT was used for data format conversion and projection transformation; the Python program code was used for data synthesis; and the ArcGIS software was used for cutting. With data processing, the monthly surface temperatures within the study area were obtained (Table 1).

Table 1. MODIS products used in this study.

RS Data	Data Type	Satellite Orbit	Time Span	Spatial Resolution	Temporal Resolution	Data Sources
MOD16A2	monthly ET	h26v05	January 2001–December 2020	500 m	8 days	NASA
MOD16A3	annual ET	h26v05	January 2001–December 2020	500 m	1 year	NASA
MOD13A3	monthly NDVI	h26v05	January 2001–December 2020	1000 m	1 month	NASA
MOD11A2	monthly surface temperatures	h26v05	January 2001–December 2020	1000 m	8 days	NASA

2.2.4. Integrated Multi-satellite Retrievals for Global Precipitation Measurement (GPM)

Integrated Multi-satellite Retrievals for GPM (IMERG) is a level-3 product and the latest generation of multi-satellite fusion inversion precipitation data for the Global Precipitation Program. IMERG provides three types of satellite data for precipitation: Early, Late and Final versions. The Final version of IMERG, with a spatial resolution of 0.1°, was adopted in this study, which introduced more sensor data sources on the basis of the Late version, including global precipitation stations for correction. The data were obtained from the EARTHSATA website (https://disc.gsfc.nasa.gov/datasets/GPM_3IMERGDF_06/summary?keywords=IMERG (accessed on 1 May 2022)) (Table 2). Using MATLAB, Python program code and ArcGIS software, the data format conversion, projection transformation, rotation registration, cutting, data synthesis and resampling were performed. After data processing, the monthly and annual precipitation data in the study area were obtained at a spatial resolution of 500 m.

Table 2. IMERG used in this study.

RS Data	Data Type	Time Span	Spatial Resolution	Temporal Resolution	RS Data Source
IMERG	monthly precipitation	January 2001–December 2020	0.1°	1 month	NASA

2.2.5. ASTER Global Digital Elevation Model

The terrain data were obtained by the ASTER Global Digital Elevation Model (ASTER GDEM), which is the global digital elevation data product jointly released by NASA and Japan's Ministry of Economy. ASTER GDEM, a new generation of Earth observation satellites of NASA, was produced on the basis of TERRA observations, with a horizontal accuracy of 30 m and elevation accuracy of 20 m, and the data were downloaded from the EARTHDATA website (https://search.earthdata.nasa.gov/search?q=ASTER&ok=ASTER (accessed on 1 May 2022)). The data format conversion, coordinate conversion, cutting and resampling were performed by the ArcGIS software. The altitude of different areas in the study area varied greatly, which directly affected land surface temperature. Therefore, ASTER GDEM was used for the correction of LST.

2.2.6. Meteorological Station Observation Data

Meteorological station observation data were obtained from the China surface climate data daily data set (V3.0), which was requested and downloaded from the China Meteorological Data Service Centre website (http://data.cma.cn/ (accessed on 1 May 2022)). The dataset contains daily data of atmospheric pressure, air temperature, precipitation, ET, relative humidity, wind direction and speed, sunshine duration and 0-cm ground temperature elements of 699 reference and basic meteorological stations in China since January 1951. In this study, the daily data on air temperature, precipitation, ET and relative humidity from 2001 to 2020 were obtained from 12 meteorological stations in Ningxia, and the monthly and annual values were calculated (Table 3).

Table 3. Meteorological station used in this study.

Number	Station	Latitude (N)	Longitude (E)	Altitude (m)
53519	Huinong	39.22	106.77	1093.1
53612	Wuzhong	37.98	106.18	1132.2
53614	Yinchuan	38.48	106.22	1111.6
53615	Taole	38.80	106.70	1102.9
53704	Zhongwei	37.53	105.18	1226.6
53705	Zhongning	37.48	105.67	1184.4
53723	Yanchi	37.78	107.40	1350.4
53806	Haiyuan	36.57	105.65	1854.8
53810	Tongxin	36.98	105.90	1340.7
53817	Guyuan	36.00	106.27	1754.2
53903	Xiji	35.97	105.72	1917.9
53910	Liupanshan	35.67	106.20	2839.1

2.2.7. Area Data of the Yellow River Irrigated

The vector data of 14 sub-irrigated areas under the administration of the Ningxia Yellow River irrigation area were provided by Ningxia water Conservancy administration department with the format of ArcGIS shape. After the coordinate transformation and topological relationship construction, the data were used to study whether there was a difference of ET and drought index of the study area and the non-irrigated area.

2.3. Methodology

2.3.1. Theil–Sen Median Trend Analysis and Mann–Kendall Test

A Theil–Sen median trend analysis and Mann–Kendall test were combined to detect the trend of long-term data. In this study, these two methods were used to determine the trends of AET and PET in the study area from 2001 to 2020.

Theil–Sen median trend analysis is a robust non-parametric statistical trend calculation method, and the calculation formula is:

$$\beta = mean\left(\frac{x_j - x_i}{j - i}\right), \forall j > i\,, \tag{1}$$

where x_i and x_j represent the x values in years i and j. The value of $\beta > 0$ reflects an upward trend; $\beta < 0$ indicates a downward trend.

The Mann–Kendall test is a non-parametric method. Unlike other parametric tests, the Mann–Kendall test does not require samples to follow a certain distribution pattern and is disturbed by abnormal values; therefore, this method is more suitable for testing sequential variables. A Mann–Kendall test had been successfully used to test hydrological and meteorological time-series data for determining whether the data showed an upward or downward trend [22,23].

When the trends of ET (including AET and PET) are tested with a Mann–Kendall test, certain time-series ET data are regarded as a group of independently distributed samples, and the parameter Z_{px} is used as the pixel ET attenuation index. The calculations are performed as follows:

$$Z_{px} = \begin{cases} \frac{S-1}{\sqrt{Var(S)}}, & S > 0 \\ 0, & S = 0\,, \\ \frac{S+1}{\sqrt{Var(S)}}, & S < 0 \end{cases} \tag{2}$$

$$S = \sum_{i=1}^{n-1} \sum_{j=i+1}^{n} sign(x_j - x_i), \tag{3}$$

$$sign(x_j - x_i) = \begin{cases} 1, x_j - x_i > 0 \\ 0, x_j - x_i = 0 \\ -1, x_j - x_i < 0 \end{cases}, \tag{4}$$

$$Var(S) = \frac{n(n-1)(2n+5)}{18}, \tag{5}$$

where n is the number of data points. When $n \geq 8$, the statistical quantity S is approximately normally distributed. *sign* is the sign function. At a given significance level (α), if $|Z_{px}| > Z_{px(1-\frac{\alpha}{2})}$, the assumption of no trend is rejected, indicating that a great trend change in the time-series data has occurred.

Using the Theil–Sen median trend analysis and Mann–Kendall test, this study analyzed the trend of ET in the study area from 2001 to 2020, and determined the significance of the ET trend at $\alpha = 0.05$. A value of $|Z_{px}| > 1.96$ indicates that the trend has passed the significance test of 95% reliability.

2.3.2. ET Complementarity Theory

According to Bouchet and ET complementarity theory for a particular region, solar radiation is constant within a given period of time. The radiation energy mainly affects surface ET, surface temperature, and air temperature. At the watershed scale, ignoring the influence of advection, the heat balance equation in the vertical direction is as follows:

$$R = LE + Q + B_s\,, \tag{6}$$

where R is ground radiation difference; LE is ET energy consumption; E is ET; L is latent heat of vaporization; Q is turbulent heat flux between the surface and atmosphere; and B_s is the change in heat storage. Compared with other terms in long periods, B_s is much smaller

and negligible. When the surface is not moist enough, the AET consumes less energy, and the excess heat raises the air temperature and reduces the humidity, which will increase the ET. Bouchet assumed that the rate of decline in AET (δET_a) is equal to the rate of increase in PET (δET_p), and vice versa. The formula is:

$$\delta ET_a = -\delta ET_p \,, \tag{7}$$

The integral of the above equation is obtained as follows:

$$ET_a + ET_p = C \,, \tag{8}$$

where C is the integral constant determined by boundary conditions. If ET under the condition of sufficient water supply is ET_w, then $ET_a = ET_p = ET_w$ and $C = 2ET_w$, which is substituted into the Equation (8), then:

$$ET_a + ET_p = 2ET_w \,, \tag{9}$$

Observational ET in a meteorological station is identified as ET_w. Based on the *t*-test, this study verified the difference between observation ET of Bureau of Plant Industry pan (BPI pan) and the sum of AET and PET, so as to analyze the complementary relationship and spatial distribution of ET in Ningxia, which is located in the arid and semi-arid regions of the upper reaches of the Yellow River. The formulas are as follows:

$$t = \frac{\overline{2ET_s} - \overline{ET_{total}}}{\sqrt{\frac{(n_1-1)S_1^2+(n_2-1)S_2^2}{n_1+n_2}\left(\frac{1}{n_1}+\frac{1}{n_2}\right)}} \,, \tag{10}$$

$$\overline{ET} = \frac{1}{n}\sum_{i=1}^{n} ET_i \,, \tag{11}$$

$$S = \sqrt{\frac{\sum_{i=1}^{n}\left(ET_i - \overline{ET}\right)}{n}} \,, \tag{12}$$

$$ET_{total} = ET_a + ET_p \,, \tag{13}$$

where ET_s is the observation ET of BPI pan in the meteorological station; ET_{total} is the sum of AET and PET; i is the number of the year; n is the sum of the years; n_1 is the number of the observation sample in the meteorological station; n_2 is the number of MODIS product sample corresponding to the location of meteorological stations.

Based on the relationship of observed ET in meteorological stations, the complementary relationship of the pixel-level ET was analyzed. AET variation trend, $Z_{px}(ET_a)$, and PET variation trend, $Z_{px}(ET_p)$, were calculated using Equation (2). When AET and PET had the same change trend or the change trend was not obvious (it failed the significance test of $\alpha = 0.05$), the complementary relationship between AET and PET did not exist. When AET and PET had significant change (through the significance test of $\alpha = 0.05$) and their change trends were opposite, AET and PET had a complementary relationship. If the ratio of the absolute value of the change was 1, AET and PET had a strict complementary relationship; otherwise, they were asymmetrically complementary (Table 4).

Table 4. Complementarity relationship between AET and PET.

Condition	Relationship	Value
$Z_{px}(E_a)/Z_{px}(E_p) \geqq 0$	Indetermination	0
$Z_{px}(E_a)/Z_{px}(E_p) < 0$ & $\lvert Z_{px}(E_a)\rvert > 1.96$& $\lvert Z_{px}(E_p)\rvert > 1.96$	Asymmetric complementation	1
$Z_{px}(E_a)/Z_{px}(E_p) < 0$ & $\lvert Z_{px}(E_a)\rvert > 1.96$ & $\lvert Z_{px}(E_p)\rvert > 1.96$ & $\lvert Z_{px}(E_a)/Z_{px}(E_p)\rvert \approx 1$	Complementation	2

2.3.3. Proposal of EDI

Based on the complementarity theory of ET, this study first proposed EDI, which was used to reflect the drought degree through the relationship between AET and PET. Under the premise of a certain ET, the smaller AET was, the smaller the surface moisture content was, that was, the more arid; otherwise, the wetter the surface moisture was. EDI was calculated as follows:

$$EDI = \frac{ET_p - ET_a}{ET_p + ET_a}, \quad (14)$$

where ET_a is the value of AET and ranges from 0 to ET_p, which limits EDI is from 0 to 1. ET_p is the value of PET. When $ET_a = 0$, the surface is absolutely dry and EDI = 1. With the increase of ET_a, EDI becomes smaller. When $ET_a = ET_p$, the supply of water is sufficient that the surface is absolute wet, and EDI = 0.

According to Equations (8) and (14) can be converted to:

$$EDI = \frac{2ET_p - C}{C}, \quad (15)$$

or

$$EDI = \frac{C - 2ET_a}{C}, \quad (16)$$

Equations (15) and (16) indicate that, in the case of fixed energy, the degree of surface aridity needs only one parameter (ET_a or ET_p) to reflect the degree of surface drought.

3. Results

3.1. Trend of Spatiotemporal Variation in AET and PET

Between 2001 and 2020, the maximum and minimum values of annual AET were 802 and 170 mm, respectively, and the average annual AET was 318 mm (Figure 2a). The Liupan Mountain in the south showed the highest AET, followed by the Yellow River irrigation area, non-irrigated area and lastly the Helan Mountain in the north. During the same time period, the maximum and minimum values of annual PET were 2050 mm and 1315 mm, respectively, and the average PET was 1584 mm (Figure 2b). Helan Mountain showed the highest PET, followed by the central plain region, and lastly the Liupan Mountain.

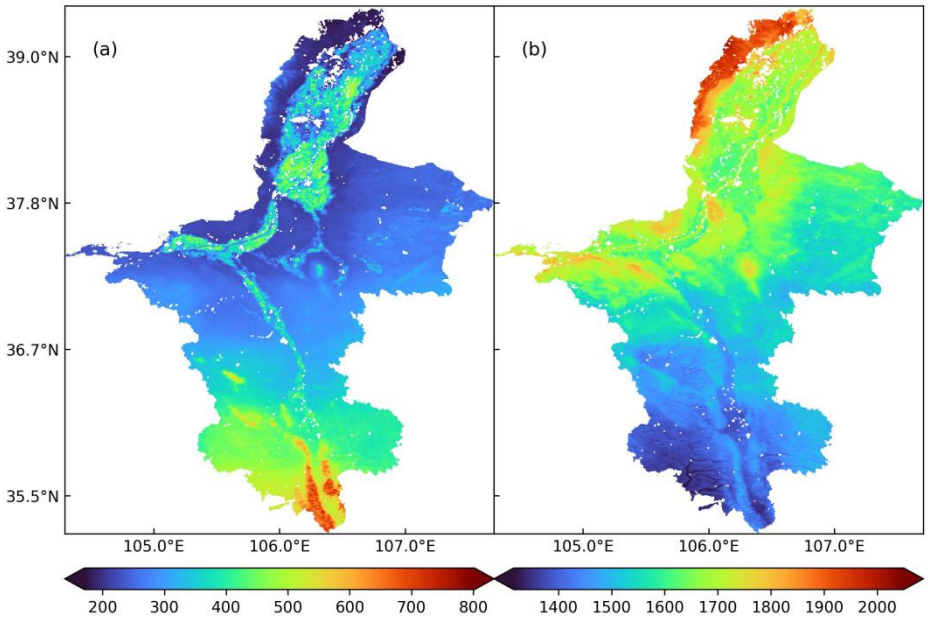

Figure 2. Assessment of annual average AET and PET in Ningxia from 2001 to 2020. (**a**) Annual average AET. (**b**) Annual average PET.

According to the Theil-Sen median trend analysis and the Mann-Kendall test, both AET and PET showed trends of significant change in the past 20 years. At the confidence degree $\alpha = 0.05$ test, the variation trend of AET, PET and the sum of AET and PET were summarized in Table 5. In the study area, AET showed a significant increase in 94.6% of the total area, no significant change in 5% of the total area and a significant decrease in 0.4% of the total area. By contrast, PET showed a significant decrease, no significant change, and significant increase in 93.5%, 6.3% and 0.2% of the total area, respectively. To verify the complementary relationship between AET and PET, we analyzed the variation trend of the sum of AET and PET. The results revealed no significant change in the sum of AET and PET in 75.5% of the total area, a significant decrease in the sum of AET and PET in 21.8% of the total area, and a significant increase in only 2.7% of the total area in the past 20 years. The areas showing a decrease or no change in AET were mainly concentrated in the Yellow River irrigation area (Figure 3a). By contrast, the areas showing no change in PET were dispersed, mainly distributed in the regions of the Helan Mountains (Figure 3b). The regions with significantly decreased ET were mainly concentrated in the central arid zone and in the southwest region of Yinchuan (Figure 3c).

Table 5. Variation trend of AET, PET and the sum of AET and PET.

ET_a			ET_p			$ET_a + ET_p$		
Trend	**Value**	**Area**	**Trend**	**Value**	**Area**	**Trend**	**Value**	**Area**
Upward	1	94.60%	Upward	1	0.20%	Upward	1	2.70%
Unvaried	0	5%	Unvaried	0	6.30%	Unvaried	0	75.50%
Downward	−1	0.40%	Downward	−1	93.50%	Downward	−1	21.80%

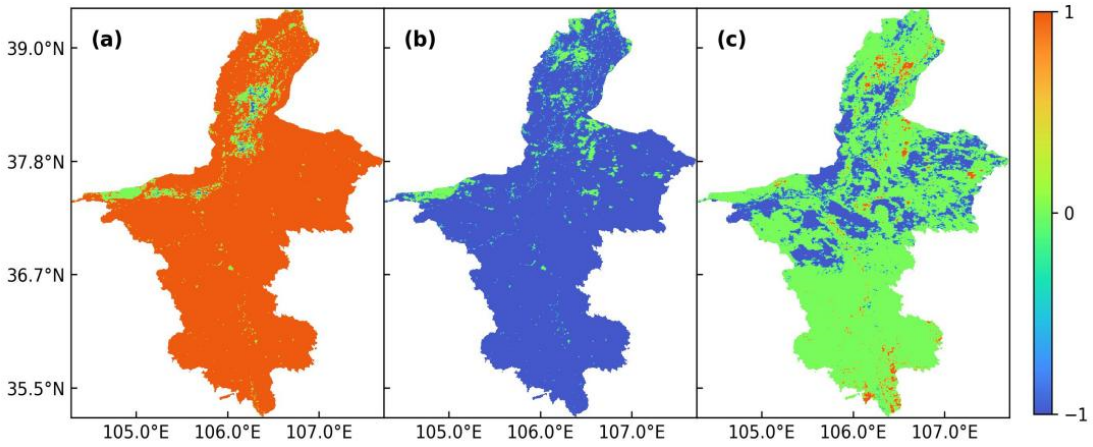

Figure 3. Trends of spatial variation in AET, PET and the sum of AET and PET in Ningxia from 2001 to 2020. (**a**–**c**) Spatial distribution of AET (**a**), PET (**b**) and the sum of AET and PET (**c**) trends.

3.2. Validation of ET Complementarity

3.2.1. Point Scale Verification

The observations of ET of BPI pan, MODIS AET and PET in the past 20 years at six meteorological stations are listed in Table 6. The *t*-test was performed on the sum of AET and PET and 2 times the measured data of BPI pan by using Equation (10), and the resulting *p*-value (0.854) indicated no significant difference between the sum of AET and PET and two times the measured data of BPI pan, therefore it could be concluded that $2ET_s = ET_a + ET_p$.

Table 6. Observations of BPI pan (ET_s), MODIS AET (ET_a) and MODIS PET (ET_p) over the past 20 years at six meteorological stations in Ningxia (mm).

Year	Taole			Wuzhong			Yanchi		
	E_s	ET_a	ET_p	ET_s	ET_a	ET_p	ET_s	ET_a	ET_p
2001	1048.2	194.8	1786.9	1073.3	179.1	1844.7	1077.4	192.3	1752.3
2002	1181.2	218.7	1776	1174.8	224.2	1791.7	1142.9	227	1697.6
2003	1086	233.4	1694.4	1145.8	195.9	1746.6	1182.8	247.4	1631.7
2004	901	226.2	1757.4	935.5	154.2	1842.4	841.6	206.7	1751.6
2005	834.6	203	1784.2	919.1	160.8	1840.8	843.8	214.5	1689.1
2006	928.4	218.4	1780.9	984.9	165.4	1843.8	917.5	204.8	1720.2
2007	967.2	265.9	1694	1013.7	221.8	1745.2	976.7	236.9	1677
2008	1076.3	228.8	1692	959.6	190.6	1762	934.4	229.6	1633.5
2009	1080.1	242.3	1666.6	919.1	202.8	1757.4	956.5	236.7	1623.4
2010	1084	283	1642.1	1020.6	245.9	1689.5	922.5	281	1599.6
2011	1103.4	301.9	1587.5	1121.8	235.3	1642	1019.2	262.9	1533
2012	877.5	294.3	1661.9	906.7	233.7	1743.3	996.3	264	1615.4
2013	807.5	271.4	1727.5	797.3	220.2	1796.5	904.8	272.8	1620.9
2014	898	370.3	1516.1	951.1	254.7	1673.8	927.4	291.4	1560.9
2015	979.1	301.6	1665.3	976.4	245.6	1738.8	1034.3	271.2	1602.7
2016	978.9	372	1627.5	976.6	282.8	1695.4	1056	307.3	1580.2
2017	889	347.6	1617.4	862.7	290.6	1675.7	971.8	320	1560.7
2018	888.9	316.5	1643.6	854.2	265.8	1719.4	965.5	299.3	1584.6
2019	856	332.4	1612.2	866	280.3	1696	934	309.9	1559.7
2020	913.3	293.5	1723.4	883.1	224.2	1823.4	1023.7	250	1669
Year	**Yinchuan**			**Haiyuan**			**Tongxin**		
	ET_s	ET_a	ET_p	ET_s	ET_a	ET_p	ET_s	ET_a	ET_p
2001	1073.3	179.1	1844.7	1168.3	275.1	1571.8	1186.9	211	1668
2002	1174.8	224.2	1791.7	1225.9	314.3	1564.4	1177.7	226	1673.2
2003	1145.8	195.9	1746.6	1300.2	354.8	1429	1208.8	277	1541.4
2004	935.5	154.2	1842.4	935.2	282.6	1583.4	835.5	212.1	1700.2
2005	919.1	160.8	1840.8	975.7	311.4	1485.7	850.8	230.9	1606.4
2006	984.9	165.4	1843.8	1025.9	283.8	1540.4	959.3	222.3	1645.6
2007	1013.7	221.8	1745.2	1141.1	336.3	1469.5	1033	257.6	1584.7
2008	959.6	190.6	1762	1082.5	292.6	1477.6	1004.8	231.7	1594.6
2009	919.1	202.8	1757.4	1129.6	317.6	1456.4	1080.3	246.7	1592.8
2010	1020.6	245.9	1689.5	1220.2	397.9	1420.7	1144.7	289.6	1543.5
2011	1121.8	235.3	1642	1322.9	389.9	1350.4	1132.8	283.5	1474.2
2012	906.7	233.7	1743.3	1223.4	370.5	1405.4	964.9	294.4	1529.2
2013	797.3	220.2	1796.5	1082.4	377.3	1461.1	867.8	291.6	1577.5
2014	951.1	254.7	1673.8	1154	395.4	1343.4	1032.1	320.1	1472.6
2015	976.4	245.6	1738.8	1068.8	389	1412.7	991.9	300.4	1522.2
2016	976.6	282.8	1695.4	1081.8	380.1	1439.9	953.7	321.7	1545.1
2017	862.7	290.6	1675.7	1049.7	393.5	1421.9	939.8	327.8	1506.9
2018	854.2	265.8	1719.4	1133.1	400	1427.5	917.6	305	1523.5
2019	866	280.3	1696	1054	416.5	1421.4	965	323.3	1522.2
2020	883.1	224.2	1823.4	1086.9	359.5	1465.4	982	264.1	1602.3

Based on complementarity theory and a modified Mann-Kendall test, the trend analysis and significance test of AET and PET were carried out on each meteorological station through Equation (7). As shown in Figure 4a,b, the AET and PET of each station conformed to a complementarity relationship. The AET and PET of three stations (Taole, Wuzhong, and Yinchuan) conformed to a strict complementarity relationship, and the other stations reflected asymmetric complementarity. As shown in Figure 4c, the AET of each meteorological station had a trend of continuous increase, and PET had a continuous decrease trend from 2000 to 2020.

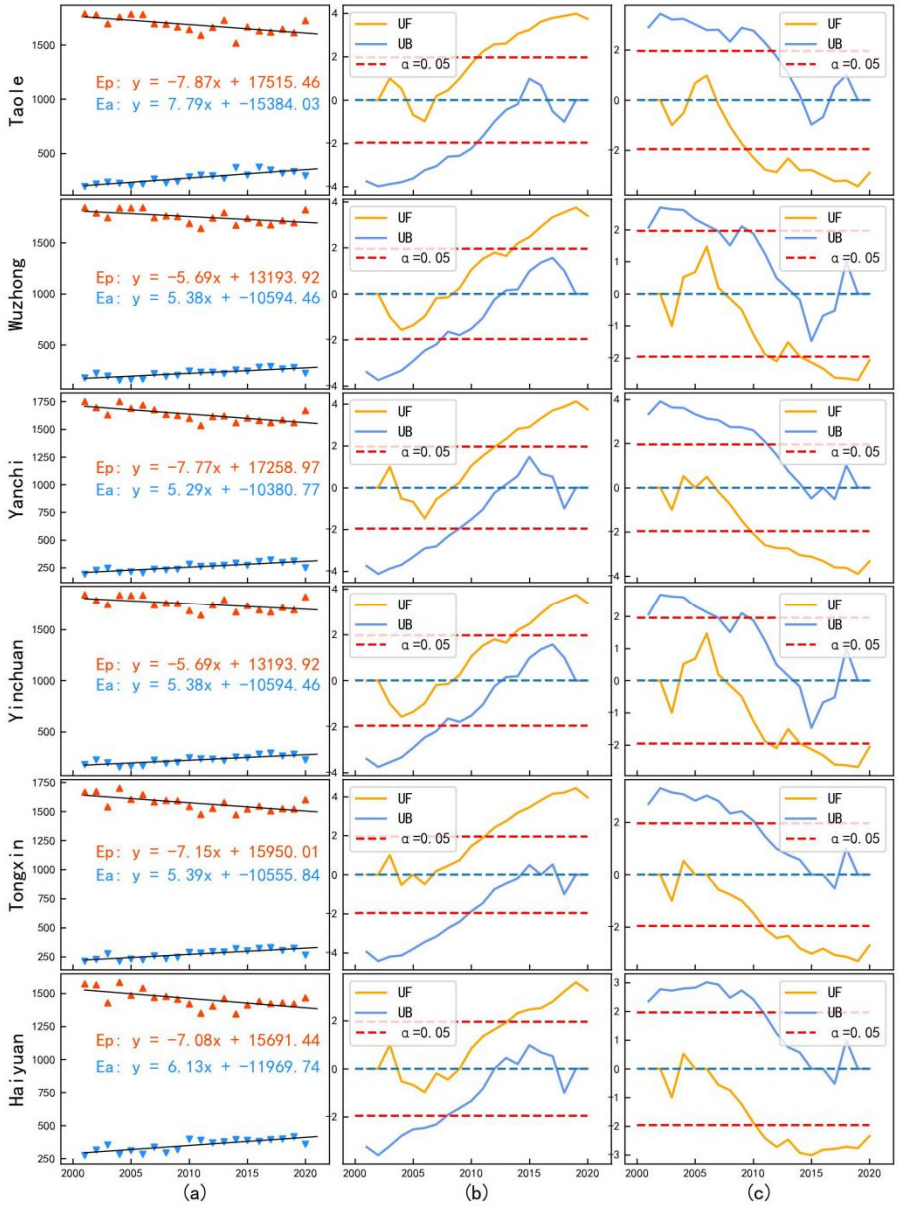

Figure 4. Trend of variation of AET (ET_a) and PET (ET_p), and Mann-Kendall test result. (**a**) Variation trends of AET and PET; (**b**) Mann-Kendall test result of AET; (**c**) Mann-Kendall test result of PET.

3.2.2. Regional Scale Verification

The *t*-test was performed on AET and PET of the study area, and passed the inspection with the confidence degree $\alpha = 0.05$. As shown in Table 7, AET and PET had strict complementarity in 69.2% of the total area in the study area, asymmetric complementarity in 21.9% of the total area and unclear regional complementarity in 8.8% of the total area. As shown in Figure 5, the regions with indeterminate complementarity were mainly located in irrigated areas along the Yellow River and in the north of Helan Mountain. The regions with asymmetric complementation were mainly distributed in the central arid zone, and most of the south regions were strict complementarity.

Table 7. Types of complementary relationship between AET and PET in Ningxia.

Complementary Relationship	Value	Area
Indetermination	0	8.80%
Asymmetric Complementation	1	21.90%
Complementation	2	69.20%

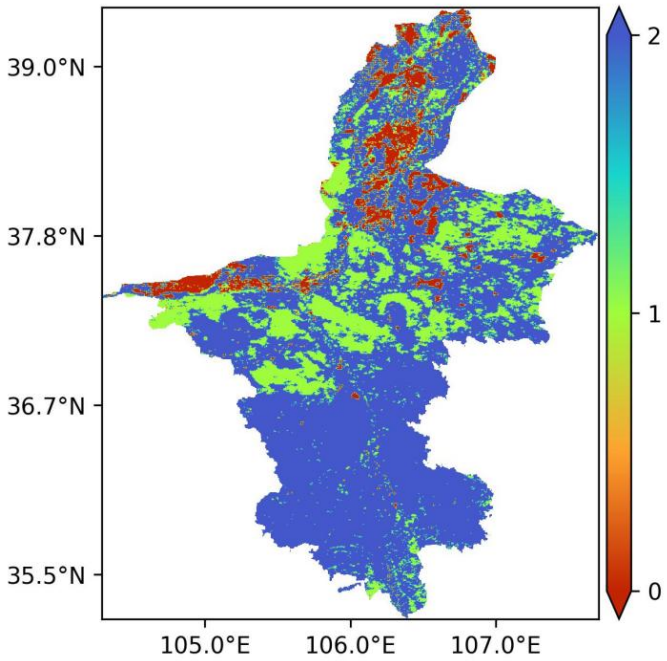

Figure 5. Spatial distribution of the complementary relationship between AET and PET.

3.3. EDI

Based on MOD16A3, the average annual EDI of the study area was calculated by Equation (14) and the pixel statistics showed that annual EDI ranged from 0.28 to 0.83, and the average EDI was 0.66. As shown in Figure 6a, the annual EDI gradually increased from the south to north, with a minimum in the Liupan Mountains in the south and a maximum in the Helan Mountains in the north. Moreover, at the same latitude, the annual EDI in the Yellow River irrigated area was smaller than that in the non-irrigated area.

The variation trend of EDI is shown in Table 8. Passing the inspection wholly with the confidence degree $\alpha = 0.05$, only 0.2% of the total area showed an upward trend of EDI; no significant change in EDI was detected in 4.7% of the total area, while 95.1% of the total area had downward in EDI. As shown in Figure 6b, except the Yellow River irrigation area, all regions showed a downward trend of EDI, which was consistent with the trend of AET change (Figure 3a).

Based on MOD16A2, monthly EDI of the study area was calculated by Equation (14). As shown in Figure 7, the monthly EDI showed considerable seasonality and interannual variations. The EDI was the lowest (0.30) in January. The EDI increased each month, reached a peak (0.82) in May, and then declined gradually to 0.31 in December.

The spatial distribution of average monthly EDI is shown in Figure 8. The spatial distribution of EDI was even in January and December, and the regional difference was minor. EDI showed considerable regional variability during the months of February, March, April, October and November, and the value of EDI in the north was larger than that in the south. EDI in the irrigated area was significantly smaller than that in the non-irrigated area during the period from May to September, and the difference in EDI between July and August was the largest.

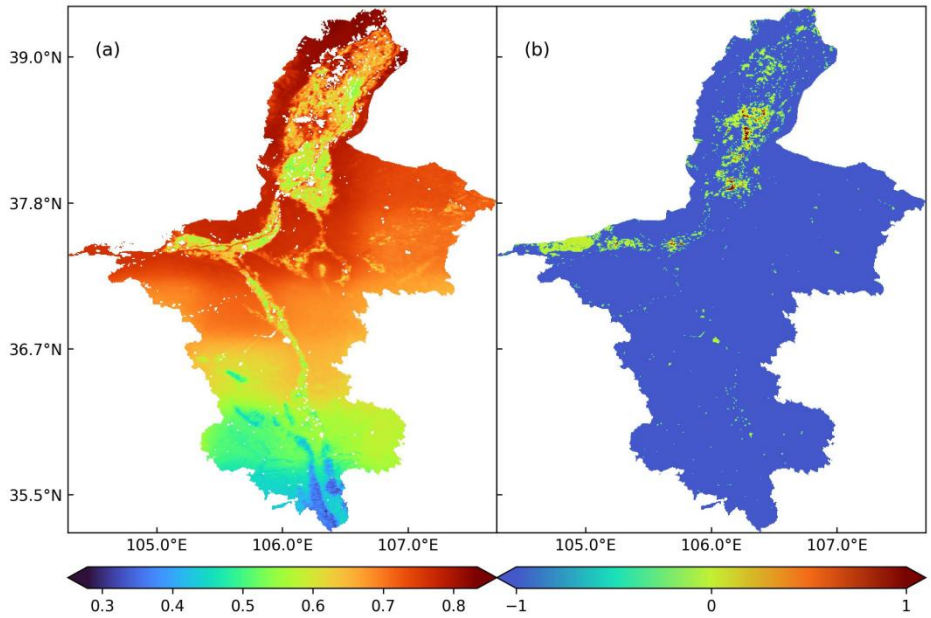

Figure 6. Evaluation of the spatial distribution patterns of average annual EDI. (**a**) Spatial distribution of average annual EDI; (**b**) Spatial distribution of EDI variation trend.

Table 8. Variation trend of EDI.

Trend	Value	Area
Upward	1	0.20%
Unvaried	0	4.70%
Downward	−1	95.10%

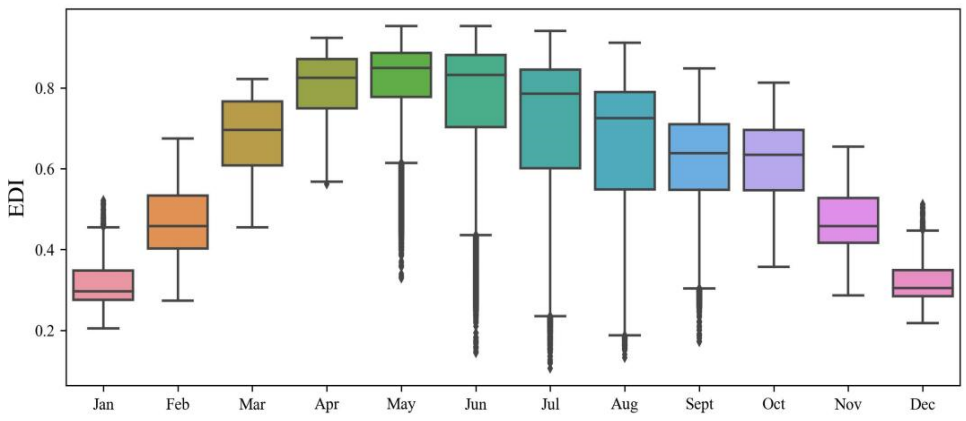

Figure 7. Temporal variation in average monthly EDI.

According to the Theil-Sen median trend analysis and the Mann-Kendall test, monthly EDI in study area showed a decrease in general except in irrigated areas (Figure 9). The most significant decrease of monthly EDI was in the southern region. With the difference of seasons, the variation trend of monthly EDI was different. The most significant decrease was in summer (June, July, August and September), and the insignificant decreasing trend was in winter that the most insignificant decreasing trend was in December. However, monthly EDI in irrigated area showed significant increasing trend from May to September which were just the irrigation time, but the change trend was consistent with the adjacent non-irrigated areas in the other months.

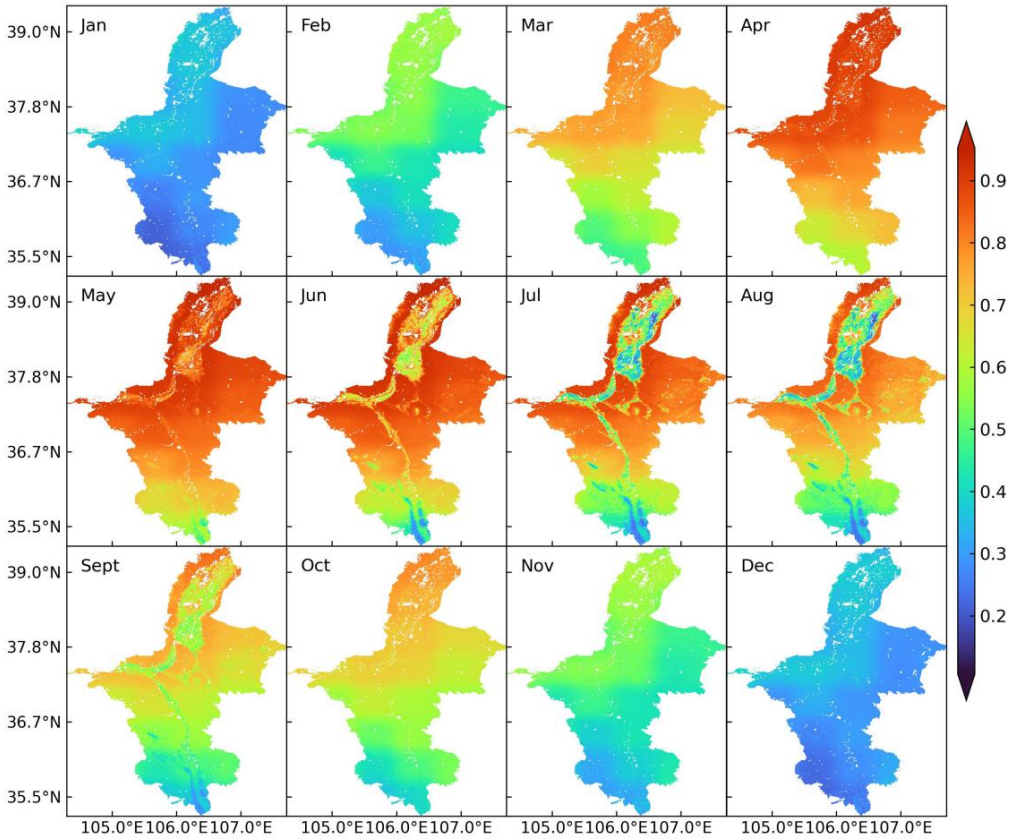

Figure 8. Spatial distribution of average monthly EDI from 2001 to 2020.

3.4. Correlation Analysis of EDI

3.4.1. Correlation Analysis on the Annual Scale

The annual precipitation in the study area ranged from 193–592 mm, while the average annual precipitation was 344 mm. As shown in Figure 10a, annual precipitation exhibited an increasing trend from northwest to southeast. The lowest precipitation was less than 200 mm in the Helan Mountains, and the highest amount was more than 500 mm in the Liupan Mountains. The annual surface temperature varied from 1 to 17 °C, with an average of 11.7 °C. As shown in Figure 10b, the surface temperature was lower in the southwest (average < 10 °C), and higher in central regions (average > 12 °C). At the same latitude, the surface temperature in irrigated areas was 1–2 °C lower than that in non-irrigated areas. The annual NDVI varied from 0.04 to 0.62, with the highest value of more than 0.5 in the Liupanshan Mountains. NDVI ranged from 0.3 to 0.4 in the irrigated area and from 0.1 to 0.2 in the non-irrigated area.

As shown in Figure 11, annual EDI showed a strong correlation with precipitation, surface temperature and NDVI in the study area from 2001 to 2020.

The maximum and minimum correlation coefficients between annual EDI and annual precipitation were 0.62 and −0.77, respectively, while the average correlation coefficient was −0.44. The negative correlation coefficient areas accounted for 96.4% of the total area, and the positive correlation areas accounted for only 1.2%, indicating that EDI and precipitation had a negative correlation in general. The spatial distribution of the correlation coefficient between EDI and precipitation (Figure 11a) showed that the regions with a positive correlation were mainly distributed in irrigated areas and the Helan Mountains, whereas those with a negative correlation were predominantly located in central and southern regions.

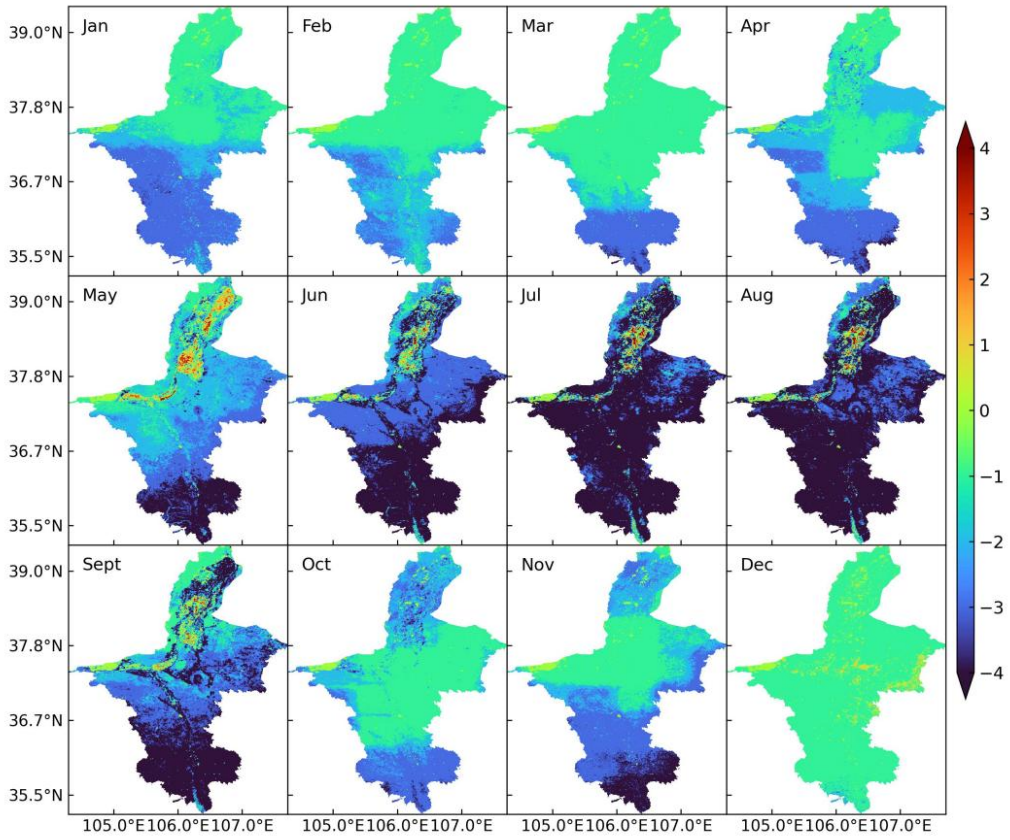

Figure 9. Trends of variation in monthly EDI. (0: no change; −1: no change; −2: insignificant decrease; −3: significant decrease; −4: extremely significant decrease; 1: insignificant increase; 2: slight increase; 3: significant increase; 4: extremely significant increase).

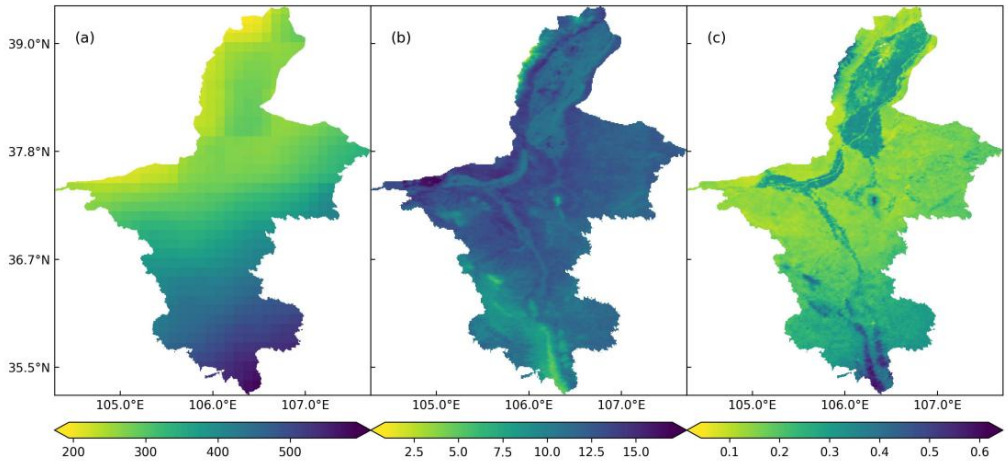

Figure 10. Spatial distribution of three influencing factors in Ningxia from 2001 to 2020. (**a**,**c**) Spatial distribution patterns of annual precipitation (**a**), annual surface temperature (**b**) and annual NDVI (**c**).

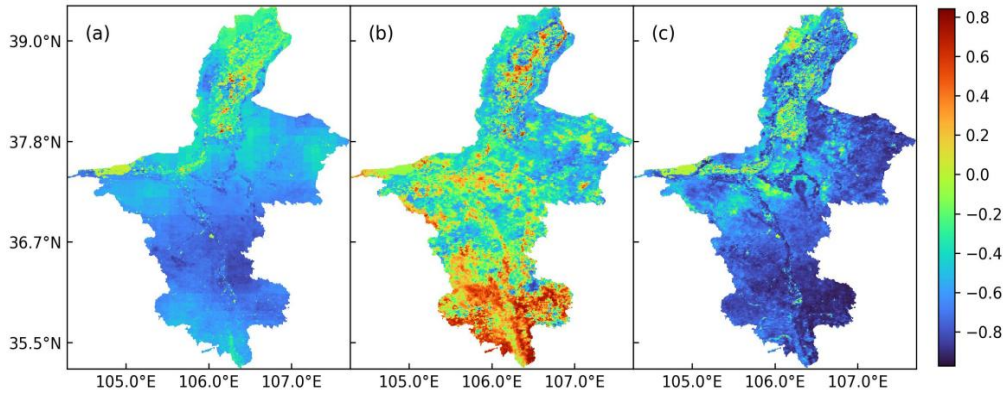

Figure 11. Spatial distribution patterns of the correlation coefficients between EDI and three influencing factors in Ningxia from 2001 to 2020. (**a**–**c**) Spatial distribution of the correlation coefficient between EDI and precipitation (**a**), surface temperature (**b**) and NDVI (**c**).

At the annual scale, the maximum correlation coefficient between EDI and surface temperature was 0.92, and the minimum was 0.89. The regions with a positive correlation coefficient accounted for 34.8% of the total area, and those exhibiting a negative correlation accounted for 62.7%. As shown in Figure 11b, the areas with a positive correlation coefficient were mainly distributed in the southern mountainous region and the Yellow River irrigated area, while those with a negative correlation coefficient were mainly distributed in the northern and eastern non-irrigated areas.

The maximum correlation coefficient between annual EDI and annual NDVI was 0.84; the minimum was −0.97; and the average was −0.66. The proportion of positive correlation coefficient areas was 1.7%, and that with a negative correlation coefficient was 95.8%, which indicated that annual EDI was negatively correlated with annual NDVI in general. As shown in Figure 11c, except the irrigated area and the Helan Mountains in the north, the correlation coefficients of all areas were negative.

3.4.2. Correlation Analysis on the Monthly Scale

According to the correlation analysis and significance test, the correlation between monthly EDI and precipitation, land surface temperature, and NDVI varied greatly in different months (Table 9).

Table 9. Correlation analysis between monthly EDI and precipitation, land surface temperature, and NDVI. (* means passing the $\alpha = 0.05$ significance test).

Month	Average Correlation Coefficient		
	Precipitation	Land Surface Temperature	NDVI
January	−0.49	0.53 *	−0.08
February	−0.13	0.35	−0.14
March	−0.66 *	0.11	−0.23
April	−0.71 *	0.13	−0.25
May	−0.43	0.34	−0.41 *
June	−0.55 *	0.12	−0.58 *
July	−0.50 *	0.29	−0.69 *
August	−0.32	0.31	−0.69 *
September	−0.35	0.34	−0.50 *
October	−0.80 *	0.19	−0.31
November	−0.74 *	0.39	−0.38
December	−0.30	0.38	−0.11

As shown in Figure 12, monthly EDI showed a negative correlation with precipitation in general, and the maximum correlation coefficient (−0.80) occurred in October and the

minimum correlation coefficient (−0.13) occurred in February. The correlation in irrigated areas was affected by irrigation time that the correlation was smaller in May to August than that in the other month.

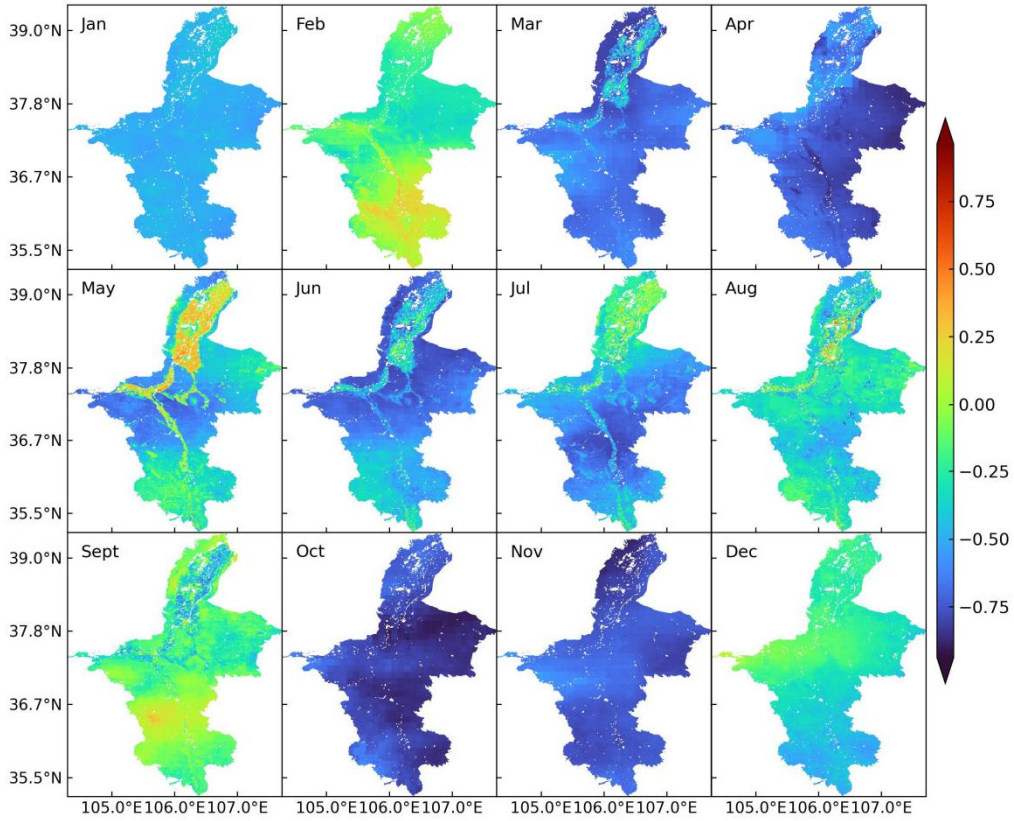

Figure 12. Spatial distribution of the correlation coefficient between EDI and precipitation.

As shown in Figure 13, monthly EDI showed positive correlation with land surface temperature in general, but the overall correlation is not high: the maximum correlation coefficient was only 0.53 in January and the minimum correlation coefficient was 0.11 in March. The correlation in the irrigated areas were significantly different than the correlation in non-irrigated areas in the irrigation period (May to August), and the difference was not obvious in the other months.

As shown in Figure 14, monthly EDI showed negative correlation with NDVI in general, and the correlation had significant seasonal differences. The negative correlation was highest in summer when plants grow better, and the maximum correlation coefficient was −0.69 in July and August. The negative correlation was lowest in winter when vegetation was sparse, and the minimum correlation coefficient was −0.08 in January. The correlation in irrigated areas and in non-irrigated areas had a great difference in May and September. At this time, monthly EDI showed an obvious positive correlation with NDVI in irrigated areas, while a negative correlation was found in non- irrigated areas. The difference was not obvious in other months.

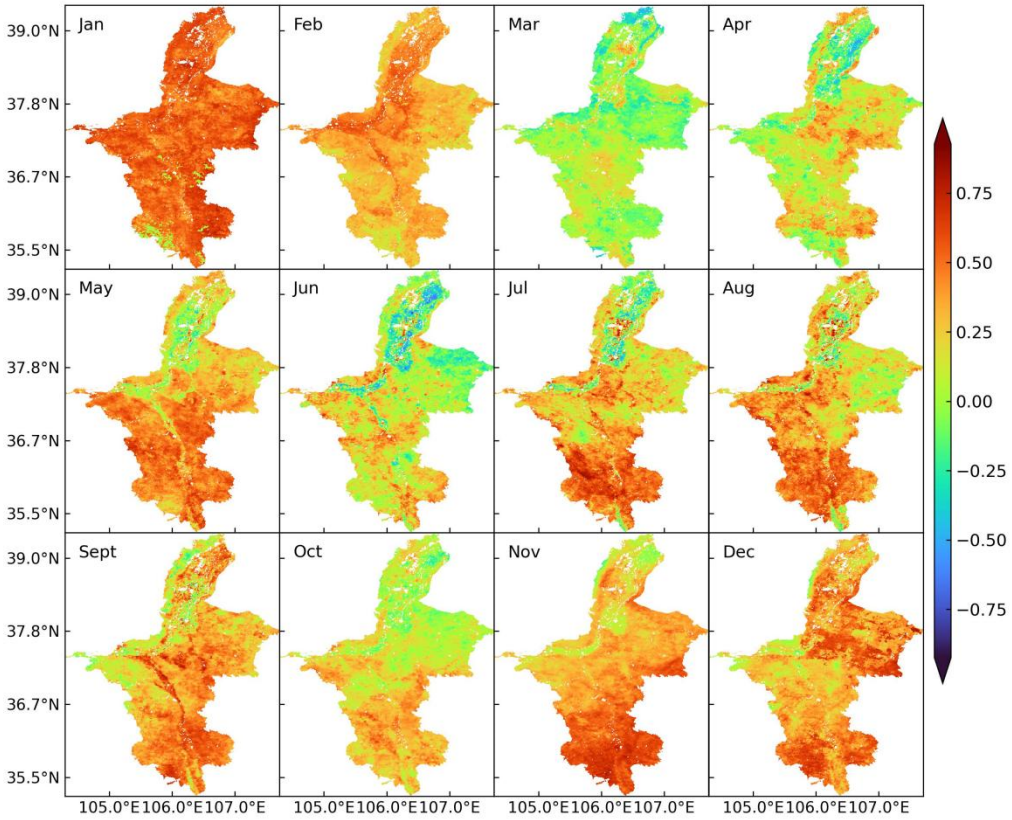

Figure 13. Spatial distribution of the correlation coefficient between EDI and land surface temperature.

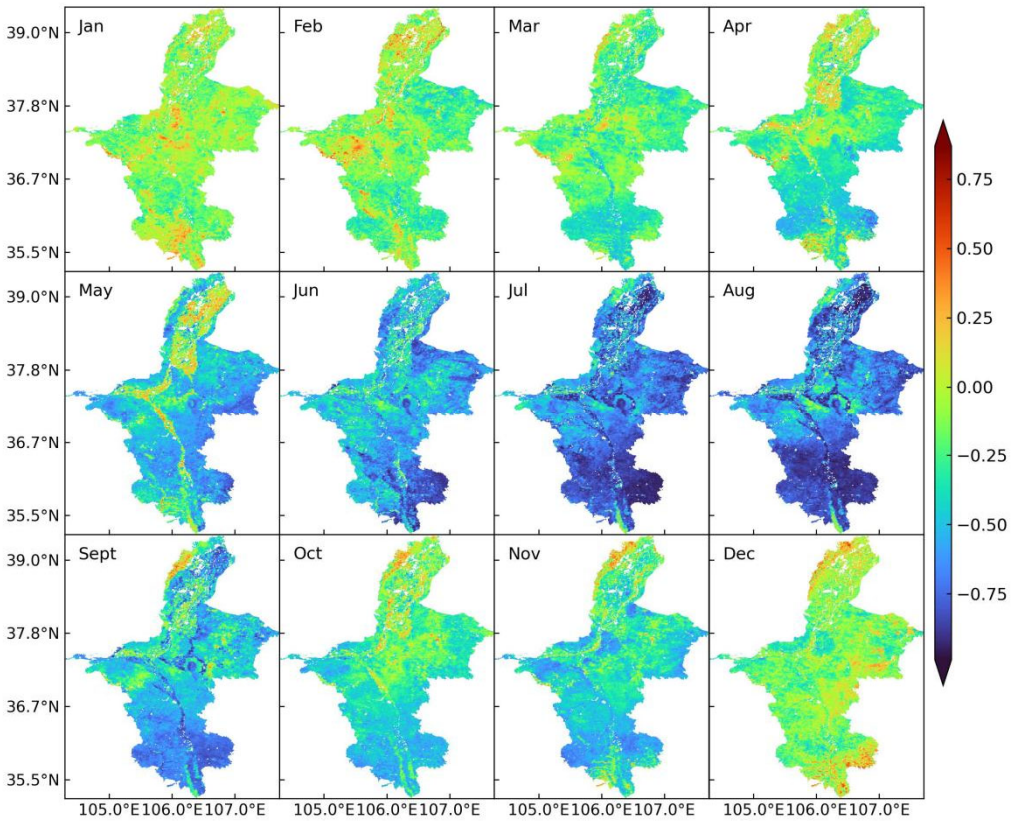

Figure 14. Spatial distribution of the correlation coefficient between EDI and NDVI.

4. Discussion

This study discovered great differences between AET and PET in Ningxia in the upper reaches of the Yellow River. The average annual AET was 20% of the average annual PET, and the minimum AET was only 9% of the minimum PET (Figure 12), which was related to the geographical location and meteorological conditions of the study area. The study area was located in arid and semi-arid areas and had little precipitation, long sunshine duration and intense radiation [21]. Among them, precipitation was the main influencing factor of AET, and radiation had a great effect on PET. The spatial distribution of AET showed that AET in irrigated areas was significantly higher than that in non-irrigated areas of the same latitude, which was mainly caused by the irrigation. The soil water content in the study area was small, but irrigation would increase the soil water content. This study showed that ET increased with the increase of soil water content in the irrigated area, which indicated that irrigation had a direct impact on AET in arid and semi-arid areas. This result was consistent with other studies [22].

In most of the study area, AET and PET had opposite trends, and the sum of AET and PET had no significant change on the whole. This result indicated that AET and PET were complementary and the complementary theory of ET was applicable in the study area. Based on the energy balance theory and ET complementarity theory, this study proposed the concept of EDI and then established an EDI model to reduce the number of the meteorological factors needed compared with those needed in previous studies. The EDI model needed only two parameters (AET and PET) or only a single parameter (AET or PET) in the case of energy determination to effectively reflect the degree of drought. Compared with the commonly used drought index $r = \frac{ET_p}{P}$ (where ET_p is PET, and P is precipitation), EDI was more accurate for reflecting drought degree, especially in arid areas. EDI not only considered the effect of precipitation, but also added the effect of non-precipitation water replenishment on the surface, such as irrigation. Under the condition of the same precipitation, irrigation would increase AET, and thus affected the degree of drought. This was verified by the fact that the AET of the irrigated area in this study area was significantly greater than that of the non-irrigated area.

It was found that the influencing factors of annual EDI and monthly EDI were quite different in the study area. The results showed that the annual average EDI of the study area was 0.66 and had a downward trend from 2001 to 2020. Many factors affected the annual EDI, and precipitation was the most sensitive factor which had a great negative correlation with EDI. The annual EDI was also affected by NDVI, land surface temperature and precipitation. According to the degree of influencing, the factors were ranked as follows: precipitation > NDVI > surface temperature. The results of correlation analysis showed that precipitation and NDVI had negative effects on annual EDI. Previous research by the authors showed that NDVI had a direct relationship with ET, which caused the change of EDI. Surface temperature had positive effect on EDI because it had a direct effect on PET. The higher of the surface temperature, the greater the PET is. Under the condition of unchanged AET or slightly changed AET, it showed from Equation (15) that the higher PET caused the greater EDI.

Monthly EDI was from 0.3 to 0.82 and its variation curve was of approximately normal distribution. The lowest monthly EDI was in January and December, and the highest was in May. The influencing factor of monthly EDI was different within seasons. The main influencing factor in winter (January, February and December) was land surface temperature. The main influencing factor in spring and autumn (March, April, May, October and November) was precipitation. The main influencing factor in summer (June, July, August and September) was NDVI. In winter, precipitation was extremely scarce in the study area, and NDVI was very small due to crop harvesting and vegetation wilt that these two factors had little influence on ET, while the change of land surface temperature was directly related to the change of surface energy, which affected the change of ET and then acted on monthly EDI. The influence of NDVI on monthly EDI was also the indirect influence of precipitation on EDI. With the increase of rainfall and temperature, NDVI

reached its maximum in summer, so the correlation coefficient between NDVI and EDI also reached its maximum in summer. NDVI in spring and autumn was smaller than that in summer, and precipitation had a greater effect on monthly EDI, and the correlation coefficient was larger.

Irrigation was the main factor responsible for monthly EDI difference between irrigated and non-irrigated regions in the study area. Due to the increase of soil moisture in the irrigated regions during the crop growing period and the transpiration of vegetation, AET was increased and then affected monthly EDI. Due to the lack of irrigation water consumption data, this study cannot take further analysis of the relationship between irrigation water consumption and drought index, but this will be one of the directions of subsequent research.

5. Conclusions

This study analyzed the spatial and temporal distribution and variation trends of AET and PET in Ningxia in the upper reaches of the Yellow River based on the MOD16 ET product; verified and confirmed the complementary relationship between AET and PET based on the measured ET data of meteorological stations; and first proposed the concept and model of EDI based on the principle of energy balance. In addition, the variation trend and influencing factors of monthly and annual EDI were also studied. The specific conclusions are as follows:

(1) The energy of ET in the study area was stable from 2001 to 2020, and AET and PET showed a complimentary relationship in the majority of regions in the study area, and most regions showed strict complementarity. The complementary theory of ET had applicability in the study area, and the results will provide a theoretical basis for further research and application of the ET model in arid and semi-arid regions.
(2) Based on the complementarity theory of ET, EDI was proposed to accurately reflect the drought in the study area at both the annual and monthly scales. EDI has the concise model and clear physical meaning that will provide technical support for drought research based on ET data.
(3) There was significant correlation between annual EDI and precipitation, land surface temperature and NDVI in the study area. The influencing factors of monthly EDI were different between the seasons. Irrigation had a great impact on the monthly EDI of irrigated and non-irrigated areas. Particularly for the irrigation period, irrigation would cause great differences between the monthly EDI of irrigated and non-irrigated areas.

Author Contributions: Conceptualization, H.L. and D.S.; methodology, H.L.; software, Z.M., J.Z. and X.W.; validation, Z.M.; formal analysis, H.L.; investigation, X.W., Y.J. and J.Z.; resources, Z.M., X.W. and J.Z.; data curation, Z.M.; writing—original draft preparation, H.L.; writing—review and editing, H.L. and D.S.; visualization, Z.M., X.W. and J.Z.; supervision, J.K.; project administration, J.K.; funding acquisition, J.K. and D.S. All authors have read and agreed to the published version of the manuscript.

Funding: This research was funded by National Natural Science Foundation of China (grant number: 42071345). This work was supported by the Department of Science and Technology of Shanxi Province Key Research and Development Projects (grant number: 2020ZDLSF06-07). This work was supported by the Key Project from National Social Science Foundation of China (Grant No: 20&ZD178).

Data Availability Statement: Not applicable.

Acknowledgments: We thank the reviewers for their suggestions.

Conflicts of Interest: The authors declare no conflict of interest.

References

1. Han, S.Z.; Zhang, B.Z. Advances of evapotranspiration research based on the Penman approach and complementary principle. *J. Hydraul. Eng.* **2018**, *49*, 9.
2. Allen, R.G.; Pereira, L.S.; Raes, D.; Smith, M. *Crop Evapotranspiration-Guidelines for Computing Crop Water Requirements*; FAO: Rome, Italy, 1998; Contract No.: 15–64.
3. Li, X.; Jiang, T.; Wu, P.; Wang, Y.; Su, B. Relationship between actual evapotranspiration and potential evapotranspiration in the Pearl River basin. *Trans. Atmos. Sci.* **2016**, *39*, 692–701.
4. Penman, H.L. Natural Evaporation from Open Water, Bare Soil and Grass. *Proc. R Oyal Soc. Lond.* **1948**, *193*, 120–145.
5. Bouchet, R. Evapotranspiration réelle et potentielle, signification climatique. *Int. Assoc. Hydrol. Sci. Publ.* **1963**, *62*, 134–142.
6. Cohen, S.; Ianetz, A.; Stanhill, G. Evaporative climate changes at Bet Dagan, Israel, 1964–1998. *Agric. For. Meteorol.* **2002**, *111*, 83–91. [CrossRef]
7. Yao, J.; Yang, Q.; Chen, Y.; Hu, W.; Liu, Z.; Zhao, L. Climate change in arid areas of Northwest China in past 50 years and its effects on the local ecological environment. *Chin. J. Ecol.* **2013**, *32*, 1283–1291.
8. Yin, Y.; Wu, S.; Zhao, D.; Zheng, D.; Pan, T. Impact of Climate Change on Actual Evapotranspiration on the Tibetan Plateau during 1981–2010. *Acta Geogr. Sin.* **2012**, *67*, 1471–1481.
9. Song, D.; Jia, B.; Jiao, H. Review of Renewable Energy Subsidy System in China. *Energies* **2022**, *15*, 7429. [CrossRef]
10. Song, D.; Liu, Y.; Qin, T.; Gu, H.; Cao, Y.; Shi, H. Overview of the Policy Instruments for Renewable Energy Development in China. *Energies* **2022**, *15*, 6513. [CrossRef]
11. Song, D.; Pei, H.; Liu, Y.; Wei, H.; Yang, S.; Hu, S. Review on Legislative System of Photovoltaic Industry Development in China. *Energies* **2022**, *15*, 306. [CrossRef]
12. Song, D.; Jiao, H.; Te Fan, C. Overview of the photovoltaic technology status and perspective in China. *Renew. Sustain. Energy Rev.* **2015**, *48*, 848–856. [CrossRef]
13. Kim, H.W.; Hwang, K.; Mu, Q.; Lee, S.O.; Choi, M. Validation of MODIS 16 Global Terrestrial Evapotranspiration Products in Various Climates and Land Cover Types in Asia. *Ksce J. Civ. Eng.* **2012**, *16*, 229–238. [CrossRef]
14. Liu, S.M.; Xu, Z.W.; Zhu, Z.L.; Jia, Z.Z.; Zhu, M.J. Measurements of evapotranspiration from eddy-covariance systems and large aperture scintillometers in the Hai River Basin, China. *J. Hydrol.* **2013**, *487*, 24–38. [CrossRef]
15. He, T.; Shao, Q. Spatial-temporal Variation of Terrestrial Evapotranspiration in China from 2001 to 2010 Using MOD16 Products. *J. Geo-Inf. Sci.* **2014**, *16*, 979–988.
16. Dong, G.; Fan, D.; Yang, T.; Xu, H.; Zhou, J.; Dang, S.; Cheng, C. Analysis on the Applicability of GPM and TRMM Precipitation Data in the Yellow River Basin. *Res. Soil Water Conserv.* **2018**, *25*, 81–87.
17. Meng, C.; Mo, X.; Liu, S.; Hu, S. Extensive evaluation of IMERG precipitation for both liquid and solid in Yellow River source region. *Atmos. Res.* **2021**, *256*, 105570. [CrossRef]
18. Li, Y.; Ning, S.; Ding, W.; Jin, J.; Zhang, Z. The evaluation of latest GPM—Era precipitation data in Yellow River Basin. *Remote Sens. Land Resour.* **2019**, *31*, 164–170.
19. Liu, X.; Li, W.; Su, Z.; Wang, S.; Li, C.; Wang, X. Change of Mean Temperature and Extreme Temperature in Ningxia during the Period of 1962–2015. *Arid. Zone Res.* **2018**, *35*, 1173–1180.
20. Li, W.; Zhao, Y.; Wang, X.; Wang, S.; Li, C.; Wang, X.; Dong, Y. Influence of water quality on element leaching of sandy compacted gravel under freeze-thaw cycle conditions. *J. Drain. Irrig. Mach. Eng.* **2020**, *38*, 506–510.
21. Ningxia Irrigation Area. Available online: http://www.yrcc.gov.cn/hhyl/yhgq/201108/t20110813_101700.html (accessed on 1 May 2022).
22. Yang, Y.; Wang, L. Variation characteristics and numerical simulation of soil water content and land evapotranspiration over farmland in the Loess Plateau. In Proceedings of the 34th Annual Meeting of the Chinese Meteorological Society, Zhengzhou, China, 26–29 September 2017.
23. Liu, H.; Song, D.; Kong, J.; Mu, Z.; Zhang, Q.; Wang, X. Spatiotemporal Variation in Actual Evapotranspiration and the Influencing Factors in Ningxia from 2001 to 2020. *Int. J. Env. Res. Public Health* **2022**, *19*, 12693. [CrossRef] [PubMed]